Progress In Electromagnetics Research Letters, Vol. 93, 99–106, 2020

An Improved Loop Ultra-Wideband MIMO Antenna System for 5G Mobile Terminals

Zhong Yu, Meng Wang*, and Yongbin Xie

Abstract—An eight-element ultra-wideband multiple-input multiple-output antenna system is proposed for the 5G mobile terminals. Each radiating branch is composed of a Loop and a monopole antenna. The ultra-wideband characteristics of the antenna are obtained by a T-shaped feed branch coupling a radiation branch. Furthermore, the isolation is lower than −15 dB by introducing a T-shaped neutralization line structure. The results of simulation and measurement show that the antenna system can cover 3.3–5.6 GHz, and the antenna efficiency is 45%–80%. At the same time, the envelope correlation coefficient between any two elements is lower than 0.03. Therefore, the proposed antenna in this study is very suitable for the eight-element MIMO antenna system as a reference.

1. INTRODUCTION

The requirements for high data transmission rates of 5G are constantly increasing in order to ensure that the fifth-generation mobile communication has a good transmission effect. Therefore, multiple-input multiple-output (MIMO) technology is particularly important [1]. MIMO technology allows to send and receive a great deal of data simultaneously. on the same wireless channel, which greatly improves the signal transmission rate. At present, mobile MIMO antenna is increasingly advocated to use 8×8 or more antenna elements [2–4]. At the same time, in the face of the high throughput encountered by 5G technology, ultra-wideband antennas can increase the channel capacity without increasing the input power [5]. Therefore, an ultra-wideband MIMO antenna has advantages in solving the above problems.

In recent years, many scholars have done a lot of researches on eight-element MIMO antennas. However, from antenna system's simulated and measured results in the literature, antennas in some papers can only cover a single frequency band. For example, in [6], an 8-element slot antenna system with dual polarizations is proposed, and the −10 dB impedance bandwidth is 3.4–3.8 GHz. In [7] an 8-element slot antenna array is proposed. The opened and closed slot dimensions are $10.8 \times 1\,\text{mm}^2$ and $28.8 \times 1\,\text{mm}^2$, respectively. Not only does the system have a narrow bandwidth (3.3–3.6 GHz), but also the size of the closed gap is large. The slots are all etched on a PCB which have an effect on the integrity of the motherboard. After further researches on the MIMO antenna, Liu et al. proposed a dual-frequency PIFA MIMO antenna system. Each antenna element was composed of two PIFA antennas. The −6 dB impedance bandwidth was 2.52–2.68 GHz (170 MHz) and 4.75–5.05 GHz (300 MHz). The antenna was placed on the PCB and took up a lot of area, which is not conducive to the design of other mobile phone circuits [8]. Ren et al. proposed a multi-band antenna system [9]. However, the frequency bands are independently separated. In [10], an 8-unit broadband MIMO antenna system was proposed, and there were three coupling parts in the antenna. Regulating the length of the coupling part, the loop antenna can work at 0.5λ, 0.75λ, 1.5λ, and finally cover 3.3–5.0 GHz. Comparing the above researches, it can be clearly seen that the loop antenna is easier to achieve broadband. Therefore, it is necessary to consider

Received 28 July 2020, Accepted 9 September 2020, Scheduled 24 September 2020
* Corresponding author: Meng Wang (1076360186@qq.com).
The authors are with the Xi'an University of Posts & Telecommunications, Xi'an, China.

using a loop antenna to design a broadband MIMO antenna system for reducing the throughput and increasing the data rate of the 5G communication system.

In this paper, an ultra-wideband MIMO antenna system that can be applied to 5G mobile terminals and can cover 3.3–5.6 GHz is proposed. Each antenna element is modified by a traditional loop antenna adding a monopole branch. At the same time, a T-shaped coupling branch is used to achieve ultra-wideband characteristics instead of the traditional Loop-type feeding method. Therefore, the size of the antenna is reduced by more than ten millimeters while covering the same frequency band. By adjusting the distance between the antennas and the T-shaped decoupling structure, the isolation between any two antennas is lower than −15 dB. At last, this paper studies the antenna pattern and calculates the envelope correlation coefficient (ECC) and antenna efficiency.

2. MIMO ANTENNA SYSTEM

2.1. Antenna Model

Figure 1(a) shows the proposed antenna system model. The antenna system is composed of 8 antenna elements which have the same shape but different dimensions. Ant 1, 4, 5, and 8 have the same size because they have the same position relative to the ground. The antenna sizes are affected by the current on the ground plane. Ant 2, 3, 6, and 7 are the same (as Table 1). The dimension of the substrate is $150 \times 75 \times 0.8\,\text{mm}^3$. Both the bottom and side frame are Fr4 substrate ($\varepsilon_\gamma = 4.4$, $\delta = 0.02$). Each antenna element is fed with a microstrip line, and the SMA connector is connected to the microstrip line through the via hole. A T-shaped decoupling structure is introduced between two adjacent antennas, and the antenna element and decoupling structure are located on the different sides of the small frame. The distances between Ant 1 and Ant 2, Ant 2 and Ant 3, Ant 3 and Ant 4 are $D12$, $D23$, $D34$, and the length of $D12 = D23 = D34$.

The detailed dimensions of the antenna element are shown in Figure 1(b). The height and length of the radiating element are $L2(H)$ and $L3$. The length of the feeding element is $L5$, and the widths are $W1$ and $W2$. The radiating element is composed of a Loop-type and a monopole branch, and the monopole antenna divides the radiating surface into two parts. The right half is the low frequency, and the left half is the high frequency.

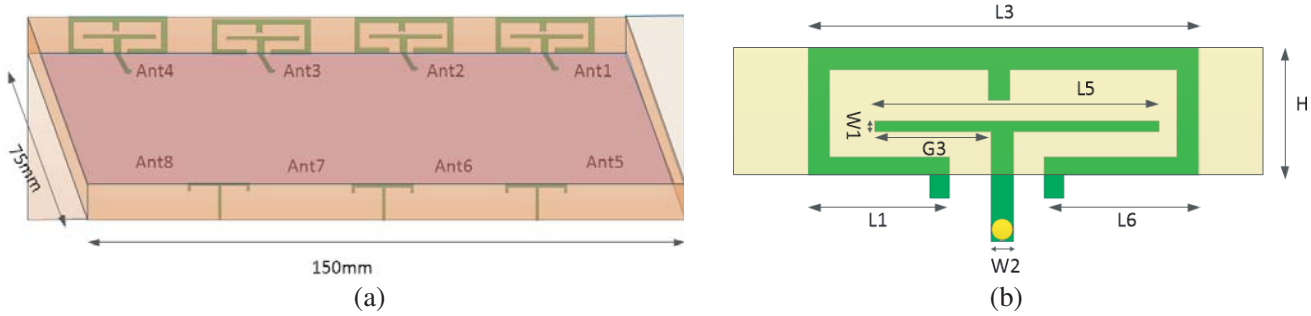

Figure 1. Geometry and detailed dimensions: (a) Overall view; and (b) antenna-element.

Table 1. The value of the optimized parameters.

Parameters	Ant 1, 4, 5, 8	Ant 2, 3, 6, 7	Parameters	Ant 1, 4, 5, 8	Ant 2, 3, 6, 7
$L1$/mm	5.5	6.3	$L2(H)$/mm	7.5	7.5
$L3$/mm	17.5	17.5	$L4$/mm	1.5	1.5
$L5$/mm	15	15.5	$L6$/mm	7.5	8
$W1$/mm	0.5	0.5	$W2$/mm	1.5	1.5

2.2. Parameters Study

In order to illustrate the working principle of the antenna, S_{11} is varied with parameters which is shown in Figure 2. It can be seen from Figure 2(a) and Figure 2(b) that $L3$ and $G3$ are the key parameters that influence the resonant points. Increasing the length of $L3$ is equivalent to increasing the length of the low-frequency part when the position of the monopole antenna remains unchanged. Therefore, $L3$ affects the first resonance point. However, it is the best choice to design $L3 = 17$ mm in order to ensure the isolation and overall size of the antenna system. Figure 2(b) shows the change of S_{11} with $G3$. T-branch coupling current of high frequency part decreases and flows to low frequency when $G3$ increases. The actual length of the coupled high-frequency part of the T-type coupling branch becomes shorter; therefore, $G3$ shifts to the right.

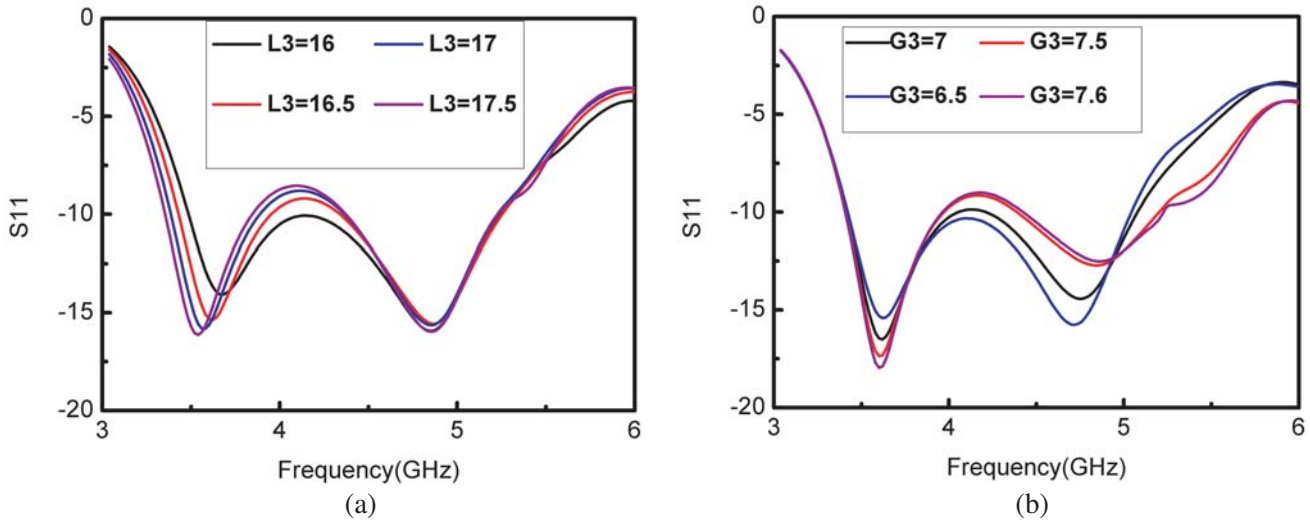

Figure 2. S_{11} varies with parameters of: (a) $L3$; and (b) $G3$.

2.3. Decoupling Structure

Figure 3 and Figure 4 show the current distributions and the transmission coefficients between Ant 1 & 2 with and without decoupling structure. From Figure 3(a), it can be clearly seen that a strong coupling occurs between Ant 1 and Ant 2 especially in the feeder part when port 1 is excited, and port 2 is not excited. The proposed decoupling structure can prevent the current flowing from Ant 1 to Ant 2. Simultaneously, the transmission coefficient has increased from -11 dB to -16 dB and even increased to -19 dB in 3.4–3.8 GHz. Therefore, the decoupling structure can reduce the coupling between the antenna elements effectively.

3. RESULTS AND DISCUSSION

According to the optimized size, the antenna system was fabricated and measured as shown in Figure 5. The actual measurement of the antenna was performed using the Agilent E5071C Network Analyzer and anechoic chamber. Since Ant 1, 2, 3, 4 and Ant 5, 6, 7, 8 are symmetrically distributed, only part of the results are analyzed.

3.1. S-Parameters

Figure 6 shows the simulated and measured S-parameters of the antenna element varied with frequency. It can be seen from Figure 6(a) that the -6 dB impedance bandwidth of the antenna system is 3.3–5.6 GHz. However, Ant 2 has frequency deviation in the high frequency part, which may be caused by dimensional deviation of the antenna model. Figure 6(b) shows the transmission coefficients between

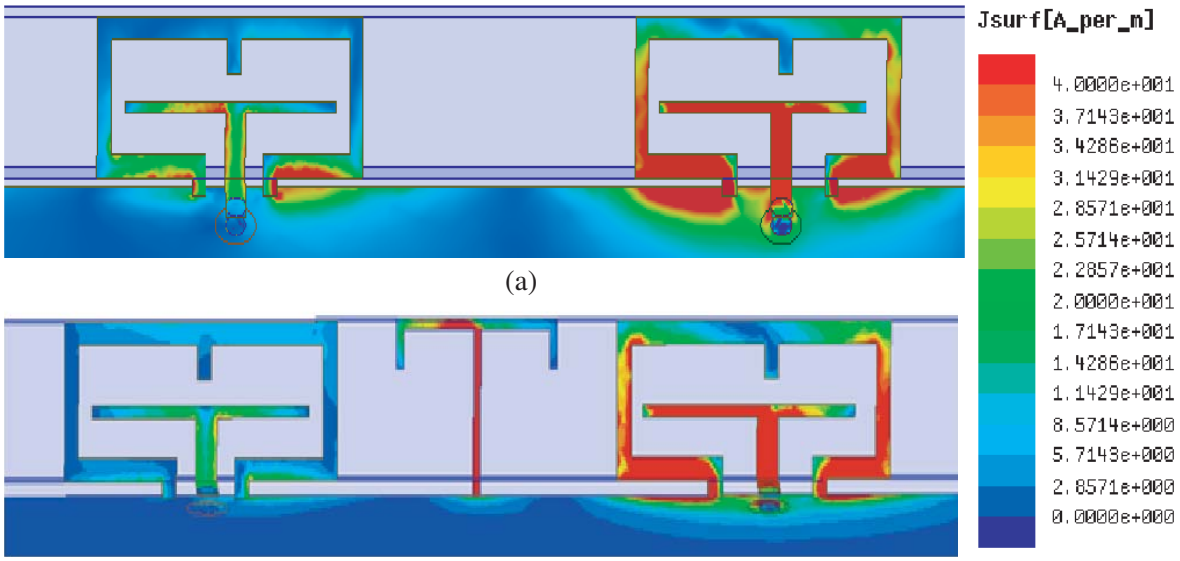

Figure 3. Current distribution on the antenna surface: (a) without decoupling structure; and (b) with decoupling structure.

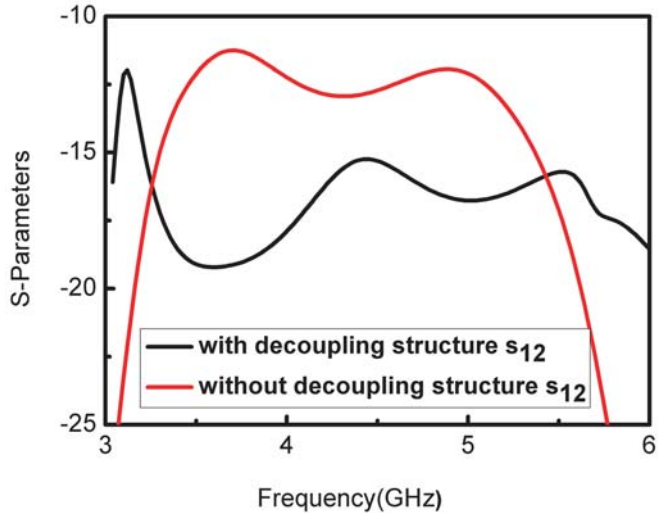

Figure 4. S_{12} with decoupling structure and without decoupling structure.

Ant 1 & 2, Ant 2 & 3, Ant 1 & 5. The isolation between any two ports is less than −15 dB in the 3.3–5.6 GHz, and the isolation of Ant 2 & 3 at 3.3–3.7 GHz is far less than −20 dB. This shows that the decoupling structure has a good suppression effect on low-frequency currents.

3.2. Radiation Performances

The radiation performance of the antenna can be reflected through the pattern. Figure 7 shows the 2D radiation patterns of Ant 1 and 2 at 3.7 GHz, 4.8 GHz, and 5.6 GHz in *xoz* and *yoz* planes. It can be seen from Figure 7 that Ant 1 and 2 show strong radiation characteristics. However, the radiation characteristics of Ant 2 on the *H* plane are slightly worse at 105°, and the reason is that the position of each antenna relative to the ground is different, and the SMA connector and measuring environment were not considered during the simulation.

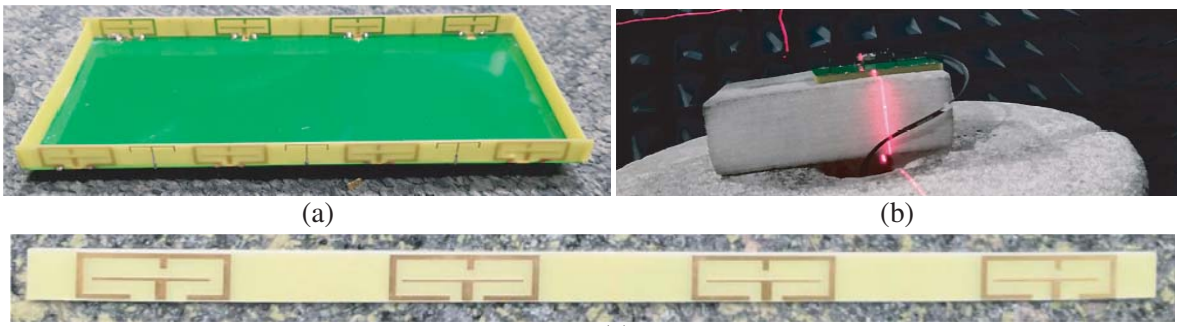

Figure 5. Photographs of: (a) the fabricated MIMO antenna system; (b) the far field experiment; and (c) side view.

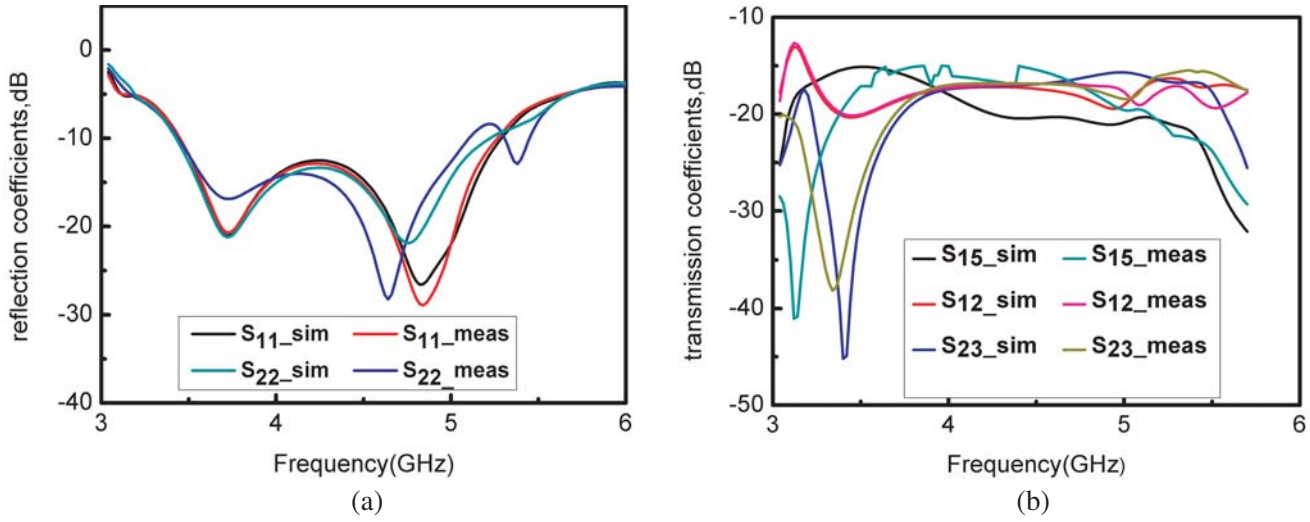

Figure 6. The S parameters: (a) reflection coefficients; and (b) transmission coefficients.

3.3. MIMO Efficiency and Performances

In this section, the efficiency and ECC will be studied. The antenna efficiency was measured in a microwave anechoic chamber. As shown in Figure 8, the efficiency of a single antenna is 45%–80% in the 3.3–5.6 GHz. ECC represents the correlation between the received signals of two antennas. It is a critical indicator to evaluate the diversity performance of a multi-antenna system, and it can be obtained from Equation (1) as [11], where q^*_{sml} represents the conjugate complex of q_{sml}, and q_{sml} is the complex coefficient of the spherical harmonic. The parameter of m describes the azimuthal variation of the field. The variation in elevation depends on degree l and order m, and index s is connected with the components of TE and TM waves. As can be seen from Figure 9, the ECC value in the covered frequency band is less than 0.03 and is close to 0 at 3.5–5 GHz; therefore, the terminal system has good diversity characteristics.

$$\mathrm{ECC} = \frac{\sum_{l=1}^{\infty}\sum_{m=-1}^{l}\sum_{s=1}^{2} q^1_{sml}\left(q^2_{sml}\right)^*}{\sqrt{\left(\sum_{l=1}^{\infty}\sum_{m=-1}^{l}\sum_{s=1}^{2} q^1_{sml}\left(q^1_{sml}\right)^*\right)\left(\sum_{l=1}^{\infty}\sum_{m=-1}^{l}\sum_{s=1}^{2} q^2_{sml}\left(q^2_{sml}\right)^*\right)}} \tag{1}$$

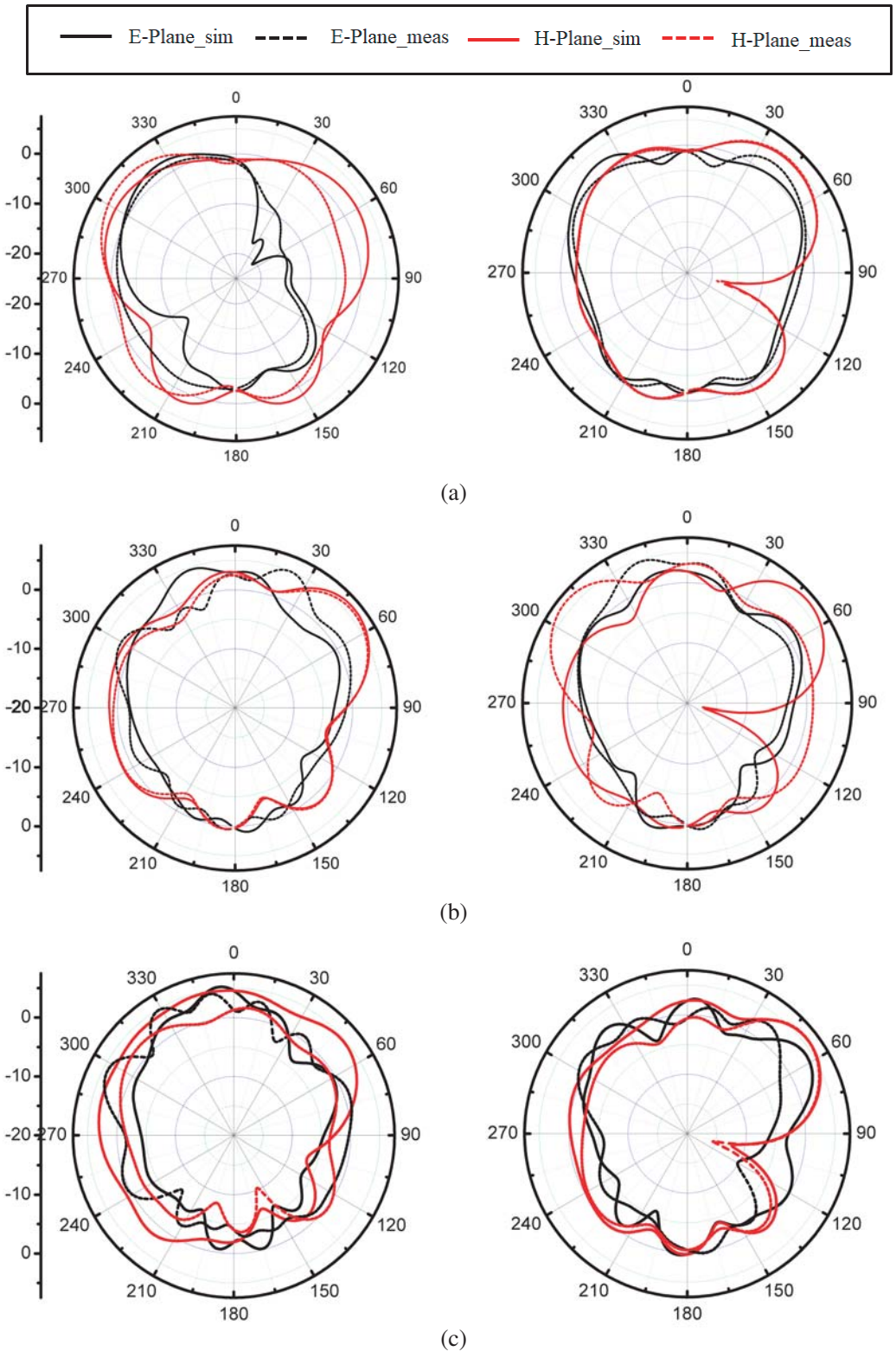

Figure 7. 2-D radiation patterns of the Ants 1, 2: (a) in the EH-plane at 3.7 GHz; (b) in the EH-plane at 4.8 GHz; and (c) in the EH-plane at 5.6 GHz.

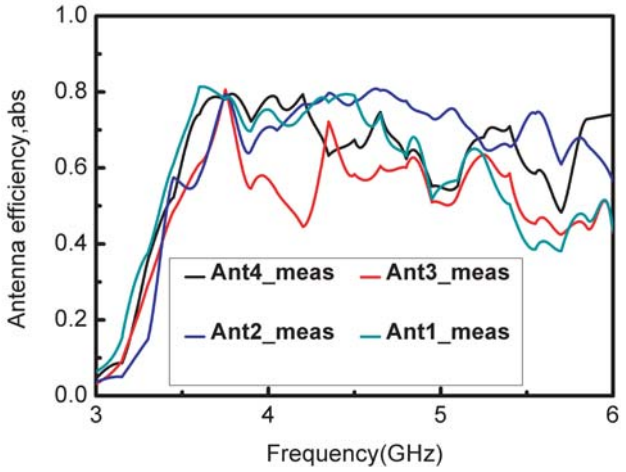

Figure 8. Measured efficiency of Ant 1, 2, 3, 4.

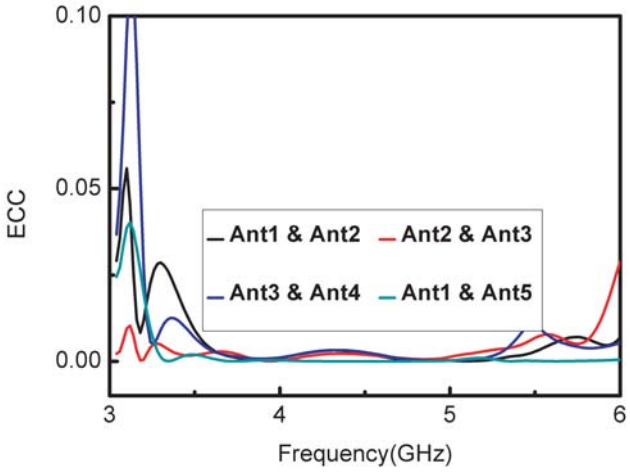

Figure 9. ECC between antennas.

Table 2. Indicators comparison with previous work.

Work	Total Size (mm^3)	Decoupling method	Impedence bandwidth (GHz)	Isolation (dB)	Antenna effectiency	ECC
Proposed	$150 * 75 * 0.8$	Neutralization line	3.3–5.6 GHz (−6 dB)	−15	45–80	0.03
[7]	$150 * 75 * 0.8$	No	3.4–3.6 (−6 dB)	−13	42–75	0.15
[10]	$150 * 75 * 0.8$	No	3.3–5.0 (−6 dB)	−14.5	46–80	0.1
[12]	$150 * 80 * 0.8$	No	3.3–4.2 (−6 dB)	−14.4	60–70	0.08
[13]	$150 * 75 * 0.8$	No	3.4–3.8 5.15–5.925(−6 dB)	−11	42–65 62–82	0.15 0.05
[14]	$150 * 75 * 0.8$	No	3.4–3.6 (−6 dB)	−17	55–75	0.1
[15]	$150 * 73 * 0.8$	Orthogonal-mode	3.4–3.6 (−6 dB)	−17	49–72.9	0.1

Compared with other studies on MIMO antennas as in Table 2 [7, 110, 12–15], the proposed antenna system has certain advantages over other studies in not only bandwidth but also ECC. The introduction of a decoupling structure in a limited space greatly reduces the coupling between the antennas. Apparently, the proposed antenna is also with high efficiency. Therefore, it is very suitable for the 8-element MIMO mobile antennas.

4. CONCLUSION

This paper proposes an 8-element ultra-wideband MIMO antenna system for 5G mobile terminals. The −6 dB impedance bandwidth is 3.3–5.6 GHz. Meanwhile, the isolation is improved from −10 dB to −15 dB by introducing a T-shaped decoupling structure between adjacent antenna elements. The antenna efficiency is 45%–80%, and the ECC is less than 0.03. The simulated and measured S parameters, antenna efficiencies, and 2D radiation patterns are all meet the characteristics of a mobile phone antenna. Consequently, the proposed antenna system has good application value for 5G mobile phone antennas.

REFERENCES

1. Andrews, J. G., S. Buzzi, W. Choi, S. V. Hanly, A. Lozano, A. C. K. Soong, and J. C. Zhang, "What will 5G be?" *IEEE Journal on Selected Areas in Communications*, Vol. 32, No. 6, 1065–1082, 2014.

2. Abdullah, M., S. H. Kiani, and A. Iqbal, "Eight element multiple-input multiple-output (MIMO) antenna for 5G mobile applications," *IEEE Access*, Vol. 7, 134488–134495, 2019 (Antenna and Propagation for 5G and Beyond).
3. Hu, W., L. Qian, S. Gao, L.-H. Wen, and W. Wang, "Dual-band eight-element MIMO array using multi-slot decoupling technique for 5G terminals," *IEEE Access*, Vol. PP, No. 99, 1-1, 2019.
4. Deng, J.-Y., J. Yao, D.-Q. Sun, and L.-X. Guo, "Ten-element MIMO antenna for 5G terminals," *Microwave and Optical Technology Letters*, Vol. 60, 2018.
5. Jensen, M. and J. Wallace, "A review of antennas and propagation for MIMO wireless communications," *IEEE Transactions on Antennas & Propagation*, Vol. 52, No. 11, 2810–2824, 2004.
6. Parchin, N. O., Y. I. A. Al-Yasir, A. H. Ali, I. Elfergani, J. M. Noras, J. Rodriguez, and R. A. Abd-Alhameed, "Eight-element dual-polarized MIMO slot antenna system for 5G smartphone applications," *IEEE Access*, 15612–15622, 2019.
7. Huang, D., Z. Du, and Y. Wang, "Slot antenna array for fifth generation metal frame mobile phone applications," *International Journal of RF and Microwave Computer-aided Engineering*, Vol. 29, No. 9, e21841.1–e21841.9, 2019.
8. Liu, D. Q., M. Zhang, H. J. Luo, H. L. Wen, and J. Wang, "Dual-band platform-free pifa for 5G MIMO application of mobile devices," *IEEE Transactions on Antennas and Propagation*, Vol. 66, 6328–6333, 2018.
9. Ren, Z., S. Wu, and A. Zhao, "Triple band MIMO antenna system for 5G mobile terminals," *2019 International Workshop on Antenna Technology (iWAT)*, 163–165, 2019.
10. Zhao, A. and Z. Ren, "Wideband MIMO antenna systems based on coupled-loop antenna for 5G n77n78n79 applications in mobile terminals," *IEEE Access*, Vol. PP, No. 99, 1-1, 2019.
11. Alieldin, A., Y. Huang, M. Stanley, S. D. Joseph, and D. Lei, "A 5G MIMO antenna for broadcast and traffic communication topologies based on pseudo inverse synthesis," *IEEE Access*, 2018.
12. Zhao, A., Z. Ren, and S. Wu, "Broadband MIMO antenna system for 5G operations in mobile phones," *International Journal of RF and Microwave Computer-Aided Engineering*, 2019.
13. Li, Y., C. Y. D. Sim, Y. Luo, and G. Yang, "Multi-band 10-antenna array for sub-6 GHz MIMO applications in 5G smartphones," *IEEE Access*, 1-1, 2018.
14. Ren, Z., A. Zhao, and S. Wu, "MIMO antenna with compact decoupled antenna pairs for 5G mobile terminals," *IEEE Antennas and Wireless Propagation Letters*, Vol. PP, 1-1, 2019, doi:10.1109/LAWP.2019.2916738.
15. Sun, L., H. Feng, Y. Li, and Z. Zhang, "Compact 5G MIMO mobile phone antennas with tightly arranged orthogonal-mode pairs," *IEEE Transactions on Antennas & Propagation*, Vol. 66, No. 11, 6364–6369, 2018.